

Observability of γ Rays from Dark Matter Neutralino Annihilations in the Milky Way Halo

Lars Bergström*, **Piero Ullio†**

Department of Physics, Stockholm University,
Box 6730, SE-113 85 Stockholm, Sweden

James H. Buckley‡

Department of Physics
Washington University
St. Louis, MO 63130, USA

December 23, 1997

Abstract

Recent advances in N-body simulations of cold dark matter halos point to a substantial density enhancement near the center. This means that, e.g., the γ ray signals from neutralino dark matter annihilations would be significantly enhanced compared to old estimates based on an isothermal sphere model with large core radius.

Another important development concerns new detectors, both space- and ground-based, which will cover the window between 50 and 300 GeV where presently no cosmic γ -ray data are available.

Thirdly, new calculations of the γ -ray line signal (a sharp spike of 10^{-3} relative width) from neutralino annihilations have revealed a hitherto neglected contribution which, for heavy higgsino-like neutralinos, gives an annihilation rate an order of magnitude larger than previously predicted.

We make a detailed phenomenological study of the possible detection rates given these three pieces of new information. We show that the proposed upgrade of the Whipple telescope will make it sensitive to a region of parameter space, with substantial improvements possible

*lbe@physto.se

†piero@physto.se

‡buckley@wuphys.wustl.edu

with the planned new generation of Air Cherenkov Telescope Arrays. We also comment on the potential of the GLAST satellite detector.

An evaluation of the continuum γ -rays produced in neutralino annihilations into the main modes is also done. It is shown that a combination of high-rate models and very peaked halo models are already severely constrained by existing data.

1 Introduction

The dark matter problem is one of the most outstanding problems confronting cosmology and astrophysics today. The question of the nature of the dark matter in the Universe is a cross-disciplinary one which may need elements of particle physics for its solution. With new observations, the possible candidates get more and more constrained.

Let us first recall that from the particle physics point of view, the theoretically preferred (Einstein-De Sitter) Universe has the simple description

$$\begin{cases} \Omega_{tot} &= 1 \\ \Omega_{\Lambda} &= 0 \end{cases} \quad (1)$$

where as usual we have introduced the normalization of the energy density to the critical density

$$\Omega \equiv \frac{\rho}{\rho_{crit}} = \frac{\rho}{1.9 \cdot 10^{-29} h^2 \text{ g cm}^{-3}}, \quad (2)$$

and Ω_{Λ} is the contribution to the energy density from a cosmological constant (or equivalently from vacuum energy).

The Einstein-De Sitter model (1) has the attractive features that it is simple, avoids finetuning, and may be explained by a period of inflation in the earliest Universe. Since Big Bang nucleosynthesis (BBN) puts an upper limit to the baryonic contribution Ω_b of [1]

$$\Omega_b h^2 \leq 0.026, \quad (3)$$

with h related to the Hubble constant H_0 by $h = H_0/(100 \text{ km s}^{-1} \text{ Mpc}^{-1})$ (observationally, h lies between 0.4 and 0.8), non-baryonic dark matter dominates the energy density by a large factor in this type of model. Indeed, there is a number of different observations on scales from dwarf galaxies and upwards which point to a larger value of Ω_{tot} than that allowed by nucleosynthesis [2]. It therefore seems that non-baryonic dark matter has to be present in substantial amounts in the Universe today.

One of the prime candidates for the non-baryonic component is provided by the lightest supersymmetric particle, plausibly the lightest neutralino χ [2]. Supersymmetry seems to be a necessity in superstring theory (or M-theory) which unites all the fundamental forces of nature, including gravity. In most versions of the low-energy theory there is a conserved multiplicative quantum number, R-parity, which makes the lightest supersymmetric particle stable. Thus, pair-produced neutralinos in the early Universe which left thermal equilibrium as the Universe expanded should have a non-zero relic

abundance today. If the scale of supersymmetry breaking is related to that of electroweak breaking, Ω_χ may come out in the right order of magnitude to explain the non-baryonic dark matter.

In addition, neutralinos are generically found to decouple at a temperature that is roughly $M_\chi/20$, which means that they are non-relativistic already at decoupling and certainly behave as Cold Dark Matter (CDM) by the time of matter dominance and structure formation. Most analyses of large scale structure formation in the Universe indeed find that CDM models (perhaps with a small addition of, e.g., massive neutrinos) give the best description of observational data.

Although accelerators like the Tevatron at Fermilab and LEP at CERN have already started to probe regions of parameter space, so far without finding any supersymmetric signals, the constraints imposed are not yet very restrictive. Adding the requirement that neutralinos make up most of the dark matter, one finds that there are viable models in the mass interval $30 \text{ GeV} \lesssim M_\chi \lesssim 10 \text{ TeV}$. In the low mass range, the direct detection at accelerators or in terrestrial detectors sensitive to the weak interactions generated by χ particles of the Milky Way halo as they pass the Earth are probably the most promising methods of detection (see [3] for an extensive review).

At the high mass end (or, depending on halo parameters, maybe even over the full mass range) indirect detection methods are competitive. The best indirect signals are given by neutrinos from the Sun or the central region of the Earth, and by almost monoenergetic γ rays lines originating from neutralino annihilations in the Milky Way halo.

Neutrinos can escape from the centre of the Sun or Earth, where neutralinos may have been gravitationally trapped and therefore their density enhanced. Gamma rays may result from loop-induced annihilations $\chi\chi \rightarrow \gamma\gamma$ [4] or $\chi\chi \rightarrow Z\gamma$ [5].

The rates of these processes are difficult to estimate because of uncertainties in the supersymmetric parameters, cross sections and halo density profile. However, in contrast to other proposed detection methods they have the virtue of giving very distinct, “smoking gun” signals: high-energy neutrinos from the centre of the Earth or Sun, or monoenergetic photons with $E_\gamma = M_\chi$ or $E_\gamma = M_\chi(1 - m_Z^2/4M_\chi^2)$ from the halo. The neutrino signal has been thoroughly discussed in the literature [6]. In this article, we concentrate on γ ray lines, where three recent lines of development have prompted us to take a new look at this process (for early studies, see [7]).

Firstly, a number of numerical studies using N-body simulations [8, 9, 10, 11] have shown that in CDM cosmologies the hierarchical way that halos

form means that they should have a density profile which is quite steep with a singular behaviour $\sim r^{-\alpha}$ with estimates of α ranging from 0.2 to 1.7. The physics underlying this behaviour is simple: in CDM models with scale-invariant gaussian initial fluctuations small clumps go nonlinear first, where the large average background density at the early epochs means that the smallest clumps are densest. Through the amplifying action of gravity, larger regions of overdensity form by the merging of smaller substructures. Through tidal interactions the overall halo distribution gets smeared out, but near the center some of the densest clumps leave a trace in form of their high average overdensity. Taking the interplay between the CDM and baryonic parts of the halo into account, a satisfactory description of the rotation curves of even dwarf spheroidal galaxies can be achieved [12].

Since the probability for two CDM particles such as neutralinos to meet and annihilate each other is proportional to the square of the neutralino density, this enhancement near the galactic center could be of utmost importance for the γ ray line signal.

The second development concerns the calculation of the processes $\chi\chi \rightarrow \gamma\gamma$ and $\chi\chi \rightarrow Z\gamma$, which only recently were computed fully to one loop in the MSSM, the minimal supersymmetric extension of the Standard Model of particle physics [4, 5]. In these calculations it was shown that previously neglected contributions could increase the predicted rates by an order of magnitude, especially at the high-mass end of the allowed M_χ range.

In the high mass range, $M_\chi \gtrsim 250$ GeV, existing Air Cherenkov Telescopes (ACT) could already be sensitive to the γ ray lines. However, the third interesting development is the planning and construction of a new generation of ACTs which will have larger area, lower threshold and better energy resolution. This will improve substantially the discovery potential of these telescopes for supersymmetric dark matter. Also, plans are being made for a satellite-borne detector (GLAST is one of the design concepts) which can compensate a factor $\sim 10^4$ smaller area than ACTs by a larger angular acceptance, better energy resolution, lower energy threshold and longer integration time.

The plan of this article is as follows. In Section 2, we give an introduction to the MSSM and the predictions of the γ line flux. In Section 3 we discuss various halo models and their implications for the γ ray flux in ACTs from neutralino annihilations. In Section 4 we give an overview of present and planned detectors for cosmic γ rays, and in Section 5 we discuss the detection potential of several existing or upcoming ACTs. In Section 6 we discuss the discovery potential of satellite detectors, and in Section 7 we comment also on the diffuse continuum γ rays that would be produced as secondary

annihilation products if neutralinos make up a significant part of the dark matter. Finally, in Section 8 we discuss our results and give some concluding remarks.

2 Overview of MSSM Results for γ Lines

We have performed a detailed phenomenological analysis of the annihilation rate of non relativistic neutralinos into two photons and into a photon and a Z boson. The two processes, which have the experimentally significant feature of giving nearly monochromatic photons in the final state, with an energy $E_\gamma \simeq M_\chi$ and $E_\gamma \simeq M_\chi(1 - M_Z^2/4M_\chi^2)$, respectively, have been studied in Refs. [4] and [5] where for the first time a full one loop calculation of the two cross sections was performed. Considering a broad selection of MSSM models in which the neutralino is the lightest supersymmetric particle and a good dark matter candidate, the aim of this Section is to examine in which cases the two annihilation processes are important. We will compare the relative values of the cross sections in view of extracting information on the nature of the neutralino from a possible detection of one or both the gamma ray lines from neutralino annihilations in the galactic halo.

In the minimal $N = 1$ supersymmetric extension of the Standard Model four neutral spin-1/2 Majorana particles are introduced, the partners of the neutral gauge bosons \tilde{B} , \tilde{W}^3 and the neutral CP-even higgsinos \tilde{H}_1^0 , \tilde{H}_2^0 . Diagonalizing the corresponding mass matrix, four mass eigenstates are obtained:

$$\tilde{\chi}_i^0 = N_{i1}\tilde{B} + N_{i2}\tilde{W}^3 + N_{i3}\tilde{H}_1^0 + N_{i4}\tilde{H}_2^0 \quad (4)$$

The lightest of these, $\tilde{\chi}_1^0$ or simply χ , is commonly referred as the neutralino. It is useful to introduce the gaugino fraction Z_g defined as

$$Z_g = |N_{11}|^2 + |N_{12}|^2 \quad (5)$$

and classify the neutralino as higgsino-like when $Z_g < 0.01$, mixed when $0.01 \leq Z_g \leq 0.99$ and gaugino like if $Z_g > 0.99$.

The general R-parity conserving version of the MSSM is defined by 63 free parameters [3]. Some simplifying assumptions are necessary to reduce the number of parameters and get to a format which is numerically tractable (for a complete discussion of this procedure see Ref. [13, 14, 3]). In the scheme we use there are seven free parameters: the higgsino mass parameter

$$\begin{aligned}
1000 \text{ GeV} &< |\mu| < 30000 \text{ GeV} \\
1000 \text{ GeV} &< |M_2| < 50000 \text{ GeV} \\
1.2 &< \tan \beta < 50 \\
0 \text{ GeV} &< m_A < 10000 \text{ GeV} \\
100 \text{ GeV} &< m_0 < 30000 \text{ GeV} \\
-3 m_0 &< A_b < 3 m_0 \\
-3 m_0 &< A_t < 3 m_0
\end{aligned}$$

Table 1: Considered range for the free parameters in our realization of the Minimal Supersymmetric Standard Model.

μ , the gaugino mass parameter¹ M_2 , the ratio $\tan \beta$ of the vacuum expectation values of the two Higgs fields H_2^0 and H_1^0 , the mass of the pseudoscalar Higgs m_A , the sfermion mass parameter m_0 and other two soft supersymmetry breaking parameters A_b and A_t . Our analysis is based on 16 scans over this parameter space. Some of them are broad samplings in the parameters, others are dedicated to more specific portions of the parameter space that are interesting for the present purpose. Table 1 contains the maximal and minimal values for each parameter; in the given intervals, or in most cases in subintervals, μ and M_2 are scanned logarithmically, $\tan \beta$ is mostly scanned linearly and in a few scans logarithmically, while all the other parameters are varied along a linear scale. Rejecting those models that violate all known experimental bounds, we are left with a sample of about 62,500 supersymmetric models which could describe Nature. For each of these, the neutralino relic density $\Omega_\chi h^2$ has been computed using the exact treatment of resonances [15] and including coannihilations between neutralinos and charginos [16]. We restrict to those models which can give the neutralino as the main constituent of galactic halos, selecting the models which have a relic density that is in the interval $0.025 < \Omega_\chi h^2 < 1$ (the upper limit is given by the condition of not overclosing the universe, or equivalently giving a too low age of the Universe). About 22,000 models in our sample fulfill this condition and this is the selected sample that is shown in the graphs in this paper.

In Fig. 1 and Fig. 2 we show the predictions for the annihilation rate of neutralinos into two photons and into a photon and a Z boson as a function of the neutralino mass, while in Fig. 3 they are shown one versus the other.

¹The usual Grand Unification Theory (GUT) relations for gaugino masses are assumed in all the results presented, their release is not expected to give major modifications

It is useful to compare $2v\sigma_{2\gamma}$ and $v\sigma_{Z\gamma}$ as the γ line flux is proportional to these quantities (the 2 comes from the fact that there are two photons in that final state). In these figures as in all those that follow, each marker represents a model in our sample, we have however arbitrarily fixed a maximal density of points which are printed (it might be worth reminding that the point density in these kind of figures is meaningless and just depends on the way the parameter space is sampled). The visual effect is the same as drawing shaded zones but in this way we avoid the problem of deciding whether or not to include isolated points or empty sub-regions.

A common feature of $2v\sigma_{2\gamma}$ and $v\sigma_{Z\gamma}$ is that the highest values are given by very pure higgsino-like neutralinos (we have included models with Z_g as small as 10^{-6}), with a mass around 500 GeV. As it was already shown in Refs. [4] and [5], the cross sections tend to a constant value of about $10^{-28} \text{ cm}^3 \text{ s}^{-1}$ in the limit $Z_g \rightarrow 0$ and $M_\chi \gg M_W$. The higgsino-like neutralino branch starts at very high masses, where the relic density is close to 1 (coannihilations of neutralinos with the lightest chargino are crucial to show that neutralinos with masses higher than 3 TeV can be cosmologically acceptable [16]), and continues with increasing cross sections down to about 500 GeV where $\Omega_\chi h^2$ approaches 0.025. This is mainly due to the large cross section for the annihilation into a W boson pair. In fact, when this process becomes kinematically forbidden (for neutralino masses below the mass of the W boson) higgsino-like neutralinos become again cosmologically interesting candidates and, together with mixed neutralinos, again give the highest cross sections in that mass region.

Whereas for higgsino-like neutralinos $2v\sigma_{2\gamma}$ is in most cases greater than $v\sigma_{Z\gamma}$, it is generally the opposite for mixed neutralinos. For this class of neutralinos in the mass interval 100 – 500 GeV the branching ratios into the $Z\gamma$ final state is in most cases dominant over twice the branching ratio into 2γ . Another interesting feature is that over the whole mass scale the value of $v\sigma_{Z\gamma}$ for mixed neutralinos is concentrated in a band not wider than two orders of magnitude, while the values of $v\sigma_{2\gamma}$ are more homogeneously distributed over 5 to 6 decades. This is visible also in Fig. 3 where the mixed neutralino band starts at about $6-8 \cdot 10^{-29} \text{ cm}^3 \text{ s}^{-1}$ for both $2v\sigma_{2\gamma}$ and $v\sigma_{Z\gamma}$ and extends down to a value of $2v\sigma_{2\gamma}$ of $10^{-34} \text{ cm}^3 \text{ s}^{-1}$ for models that can give a $v\sigma_{Z\gamma}$ as high as $10^{-29} \text{ cm}^3 \text{ s}^{-1}$. We illustrate this point in Fig. 4 where we consider a scan of models with mixed neutralinos of masses in the range 150 – 400 GeV. In these figures we have indicated which is the class of diagrams that gives the main contribution to the cross sections (all the diagrams involved in the computation are shown in Refs. [4] and [5]). In the case of $v\sigma_{Z\gamma}$ almost always the W boson-chargino loop diagrams are

dominant over the other diagrams. For $2v\sigma_{2\gamma}$ instead, the contributions for the fermion-sfermion loop diagrams can be more frequently of the same order of magnitude as the W boson-chargino diagrams and severe cancellations can take place, with usually a small cross section when the fermion-sfermion diagrams are dominant. From Fig. 4 it is also evident that Higgs-chargino loop diagrams and Goldstone boson-chargino loop diagrams do not play a main role and this is true for all classes of neutralinos over the whole mass range.

Given the large size of our sample of scanned models, we expect the narrowness of the $Z\gamma$ band for large neutralino masses to be a real effect which could increase the discovery potential of present and future ACTs. In the heavy mass range, it may be appropriate to sum the $\gamma\gamma$ and $Z\gamma$ contributions, since to resolve the two lines an energy resolution better than around 1 % would be needed.

Gaugino-like neutralinos give cross sections that rarely exceed, for both processes, a few times $10^{-30} \text{ cm}^3\text{s}^{-1}$. In this case the cross sections are poorly correlated and the large spread in Fig. 3 is due mainly to gaugino-like neutralinos.

A final comment can be made about low mass neutralinos. Here $v\sigma_{Z\gamma}$ goes to zero at the threshold $M_\chi \rightarrow M_Z/2$ as expected because this limit corresponds to having no photon in the final state and the annihilation of neutralino pairs into a Z boson is forbidden by C parity (for clarity we have excluded models with neutralino masses lower than 70 GeV from Fig. 3). In addition, $2v\sigma_{2\gamma}$ has low values as well because the contribution from W boson-chargino loop diagrams becomes small (there is no contribution from the imaginary part and the real part is generally large only for heavy pure higgsino-like neutralinos).

3 Milky Way halo models

The photon flux from neutralino annihilation in the galactic halo critically depends on the neutralino distribution. Since the flux per unit volume is proportional to the neutralino density squared, any enhancement of the density would result in a sharp increase in the photon flux; such an enhancement is provided by dark matter radial halo profiles that are peaked towards the galactic center. In this section we will examine in detail this possibility and compute the full dependence of the flux on the galactic coordinates in some selected cases.

The mass distribution in the Milky Way and the relative importance

of its three components, the bulge, the disk and the halo, are poorly constrained by available observational data. Although the dynamics of the satellites of the galaxy clearly indicates the presence of a non-luminous matter component, a discrimination among the different radial dark matter halo profiles proposed in the literature is not possible at the time being [17]. Our approach is to assume that dark matter profiles are of a universal functional form and to infer the Milky Way dark matter distribution from the results of N-body simulations of hierarchical clustering in cold dark matter cosmologies. The predicted profiles in these scenarios have been tested to a sample of dark matter dominated dwarf and low-surface brightness galaxies which provide the best opportunities to test the spatial distribution of dark matter. Actually this field of research is in rapid evolution and slightly discrepant results have recently been presented [8, 9, 10, 11]; we will concentrate on the Kravtsov et al. profile [10] and the Navarro et al profile [9], comparing the results with the canonical modified isothermal sphere profile which is widely used in dark matter calculations.

Among the general family of dark matter halo profiles

$$\rho(r) \propto \frac{1}{(r/a)^\gamma [1 + (r/a)^\alpha]^{(\beta-\gamma)/\alpha}}, \quad (6)$$

Kravtsov et al. [10] propose a coreless profile with a mild singularity towards the galactic center with $\gamma \sim 0.2-0.4$; taking into account these two extremes, we will refer to the Ka profile as to the one which is defined by $(\alpha, \beta, \gamma) = (2, 3, 0.2)$, while the Kb profile is chosen as $(\alpha, \beta, \gamma) = (2, 3, 0.4)$. In previous work [9], Navarro, Frenk and White had obtained a cuspy profile which has $(\alpha, \beta, \gamma) = (1, 3, 1)$ (hereafter NFW profile). Both results are not in agreement with the modified isothermal distribution, $(\alpha, \beta, \gamma) = (2, 2, 0)$ (hereafter Sp profile), extensively used in the analyses of observed rotation curves, which is non singular with a core of radius $\sim a$.

There are models [18] which have a more singular behavior near the galactic center, and which would give enormously enhanced rate in that direction. However, there is observational evidence against such singularities from cluster gravitational lensing and the rotation curves of dwarf spiral galaxies [19]. On the other hand, the discrepancy between the $1/r$ central cusp of the NFW profile and the experimental data from the dwarf spheroidal DDO 154 has been explained in Ref. [12] assuming an additional component of dark baryons. Of course, also a moderately steeper profile like $1/r^{1.3}$, which is found in some simulations [20] and which has some theoretical underpinning [21], may be acceptable. That would give higher estimates than the one we use for the neutralino-induced fluxes, but we choose to be

more conservative.

We will consider only the case of spherical profiles; introducing a flattening parameter may enhance the value of the flux but the effect is not expected to be dramatic for this neutralino detection method and we prefer not to introduce another factor of uncertainty.

The normalization constant of the halo profile, which we choose as the value of the halo density ρ_0 at our galactocentric distance R_0 , the core radius a and R_0 itself are the three parameters which will be relevant to give a prediction for the gamma line flux. N-body simulations indicate that there may be a correlation between normalization constant and core radius, but we are not in the position of extracting a firm numerical prediction for the Milky Way. After choosing the functional form of the halo profile, we determine the regions in the parameter space which are allowed by the assumptions that follow below.

We follow Dehnen and Binney [17] and assume that the total mass of the galaxy inside 100 kpc is $7 \pm 2.5 \times 10^{11} M_\odot$. This estimate is obtained by combining the result of Kochanek [22] who used the observational constraints from the velocity distribution of the Milky Way's satellites, the local escape velocity of stars and the Local Group timing model, and the result inferred in Ref. [23] from the dynamics of the Magellanic Clouds and Stream. Both estimates are to some extent model dependent and this is the reason for the large error bound chosen. We then suppose that, for each matter distribution model, on average ten per cent of the total mass inside 100 kpc is due to the contributions of the disk and the bulge (value obtained from Table 4 in [17]) and derive a value for the the mass of dark matter halo inside 100 kpc

$$M_h(r < 100 \text{ kpc}) = (6.3 \pm 2.5) \times 10^{11} M_\odot \quad (7)$$

A second constraint is given in terms of the contribution of the halo to the local rotation curves which can be determined in terms of the observed value of the local rotation velocity Θ_0 and from the measurements of the contribution of the disk (which is dominant over the contribution from the bulge):

$$v_h^2(R_0) = \Theta_0^2 - v_d^2(R_0) \quad (8)$$

The IAU standard values for Θ_0 and our galactocentric distance R_0 , based on a review by Kerr and Lynden-Bell [24] in 1986, are respectively $220 \pm 20 \text{ km s}^{-1}$ and $8.5 \pm 1.1 \text{ kpc}$. The two quantities are not independent variables, their ratio is fixed by local stellar kinematic measurements of the Oort constant. In more recent estimates lower values have been obtained:

Reid [25] has found $R_0 = 7.2 \pm 0.7$ kpc, while in a very recent work Olling and Merrifield [26] has found $R_0 = 7.1 \pm 0.4$ kpc and $\Theta_0 = 184 \pm 8$ km s $^{-1}$. Even the value of the contribution of the disk to the local rotation velocity has large uncertainties and is to some extent model dependent. The value we can infer from Kuijken and Gilmore [27], and Gould [28], who examine a data set of velocities of local stars as a function of their height over the galactic plane, is in the range $v_d(R_0) = 137 \pm 16$ km s $^{-1}$. Maximum disk models can give a higher $v_d(R_0)$, while in thin disk models the value can be lower. We will accept the quoted value without considering disk models in detail. Combining the values of Θ_0 and $v_d(R_0)$ we obtain the following ranges of values of $v_h(R_0)$ for a given galactocentric distance R_0 :

$$v_h(R_0) \sim 128 - 207 \text{ km s}^{-1} \quad \text{if } R_0 = 8.5 \text{ kpc} \quad (9)$$

$$v_h(R_0) \sim 86 - 149 \text{ km s}^{-1} \quad \text{if } R_0 = 7.1 \text{ kpc} \quad (10)$$

In Fig. 5 we show, for each of the halo models considered, the regions in the plane (a, ρ_0) which are compatible with the limits given in Eq. (7) and Eq. (9), (10). A common feature of all the profiles is that the allowed regions are shifted to lower values of the core radius increasing the galactocentric distance from 7.1 kpc to 8.5 kpc. Focusing for instance on the Ka profile with $R_0 = 8.5$ kpc, the values of a and ρ_0 which are compatible with our constraints fall in an area with a diamond-like shape, where the upper left bound and the lower right bound are given respectively by the maximum and minimum values in Eq. (9), while the upper right and lower left are due to Eq. (7). A similar behavior is seen in all the other cases. For the Sp profile a core radius equal to zero is not excluded, but this is an extremely unrealistic case and we have decided to arbitrarily fix a lower value of $a = 1$ kpc.

The gamma ray flux from neutralino annihilation in the galactic halo is given by:

$$\Phi_\gamma(\psi) = \frac{N_\gamma v \sigma}{4\pi M_\chi^2} \int_{\text{line of sight}} \rho^2(l) dl(\psi) \quad (11)$$

where ψ is the angle between the direction of the galactic center and that of observation, and where $N_\gamma = 2$ for $\chi\chi \rightarrow \gamma\gamma$, $N_\gamma = 1$ for $\chi\chi \rightarrow Z\gamma$. Separating the dependence on the halo model from the part which is related to the values of the cross section and the neutralino mass, we rewrite it as

$$\begin{aligned} \Phi_\gamma(\psi) \simeq & 1.87 \cdot 10^{-11} \left(\frac{N_\gamma v \sigma}{10^{-29} \text{ cm}^3 \text{ s}^{-1}} \right) \left(\frac{10 \text{ GeV}}{M_\chi} \right)^2 \\ & \cdot J(\psi) \text{ cm}^{-2} \text{ s}^{-1} \text{ sr}^{-1} \end{aligned} \quad (12)$$

where we have defined the dimensionless function

$$J(\psi) = \frac{1}{8.5 \text{ kpc}} \cdot \left(\frac{1}{0.3 \text{ GeV/cm}^3} \right)^2 \int_{\text{line of sight}} \rho^2(l) dl(\psi). \quad (13)$$

Picking in Fig. 5, for the four halo models, a couple of values (a, ρ_0) which gives rather conservative results and choosing $R_0 = 8.5 \text{ kpc}$, we show in Fig. 6 in each case the angular dependence of the function J . The profiles have been considered valid up to the capture radius of the black hole at the galactic center which is about 0.01 pc for a mass of Sgr A* $M \simeq 10^6 M_\odot$. Modifications to Eq. (13) due presence of the black hole are in detail in the subsection below.

The maximum flux will be clearly in the direction of the galactic center. The relevant quantity for a measurement is, rather than $J(0)$, the integral of $J(\psi)$ over the solid angle given by the angular acceptance of a detector which is pointing towards the galactic center. We consider therefore the function

$$\langle J(0) \rangle (\Delta\Omega) = \frac{1}{\Delta\Omega} \int_{\Delta\Omega} J(\psi) d\Omega \quad (14)$$

where $\Delta\Omega$ is the angular acceptance of the detector. Fixing for an ACT detector a typical value of $\Delta\Omega = 10^{-3}$, in Fig. 7 we plot $\langle J(0) \rangle$ versus the core radius a for the allowed regions in Fig. 5 and for both choices of the galactocentric distance. As can be seen the NFW profile can give very high values of $\langle J(0) \rangle$ compared to the other halo models. In Fig. 8 we plot instead $\langle J(0) \rangle$ as a function of $\Delta\Omega$ for the conservative halo models shown in Fig. 6 together with the models corresponding to the maximum and minimum core radius allowed in Fig. 5 for each profile.

3.1 Effects of a central black hole

A small complication occurs when we try to compute the line-of-sight integral directly towards the galactic center. There are strong indications that a black hole of mass $\sim 10^6 M_\odot$ resides near the center of the Milky Way. The interplay between this black hole and the dark matter halo is difficult to model - certainly it is beyond the scope of this paper. One effect of the black hole, however, is to gravitationally lens γ rays that originate from behind the galactic center, in a cone of angular size on the order of that of the Einstein ring. This is given by (see, e.g., [29])

$$\theta_E = \sqrt{\frac{4GM}{c^2} \frac{D_{ds}}{D_d D_s}}, \quad (15)$$

where G is Newton's constant, M the mass of the black hole, D_{ds} , D_d , D_s are the lens-to-source, lens and source distances, respectively.

In general, for a point source, a double image is produced which usually cannot be resolved (the situation is similar to that of microlensing of MACHOs in the halo). The resulting magnification may, however, be detectable and is given by

$$\mu = \frac{u^2 + 2}{u \sqrt{u^2 + 4}}, \quad (16)$$

where $u = \beta/\theta_E$, with β the undeflected angle to the source. Since gravitational lensing is a purely geometrical effect, it is of course also operative for γ rays. Returning to our line-of-sight integral Eq. (13), we can now for angles ψ less than the Einstein angle $\theta_E(l) = \theta_0 \sqrt{(l - R_0)/l}$ (with θ_0 around 1 arcsec for $M = 10^6 M_\odot$ and $R_0 = 8.5$ kpc) split the integral into two parts, from 0 to the distance of the galactic center R_0 and from R_0 to the end of the halo. The second part contains the amplification factor $\mu(l)$, thus for small angles we replace $J(\psi)$ by $K(\psi)$ where

$$K(\psi) = \frac{1}{8.5 \text{ kpc}} \cdot \left(\frac{1}{0.3 \text{ GeV/cm}^3} \right)^2 \cdot \left[\int_0^{R_0} \rho^2(l) dl(\psi) + \int_{R_0}^\infty \rho^2(l) \left[\frac{\left(\frac{\psi}{\theta_E(l)} \right)^2 + 2}{\left(\frac{\psi}{\theta_E(l)} \right) \sqrt{\left(\frac{\psi}{\theta_E(l)} \right)^2 + 4}} \right] dl(\psi) \right]. \quad (17)$$

In Fig. 6 this expression has been used for the smallest angles displayed. As can be seen, it causes a mild enhancement for the most non-singular halo models and cannot compensate the turnoff of the rise of the *NFW* profile due to the black hole itself.

4 Present and Planned ACT Detectors

The present high energy gamma-ray experiments, the *Energetic Gamma-Ray Experiment Telescope* (EGRET) and the Whipple 10m atmospheric Cherenkov Telescope (e.g. [30]), lack the sensitivity to detect the annihilation lines fluxes predicted for most of the allowed supersymmetric models and halo profiles. Our aim is to show that the order of magnitude improvement in the flux sensitivity and the substantial improvements in angular resolution in the next generation of both ground based and satellite gamma-ray experiments, will allow to explore large portions of the MSSM parameter

Table 2: Characteristics of Atmospheric Cherenkov Telescopes[†]

	Whipple	GRANITE-III	VERITAS or HESS
Effective Area (cm ²)	3.5×10^8	5×10^8	7×10^8
Energy Resolution (σ_E/E)	30%	20% ^a	15% ^b
Angular Resolution (σ_θ)	0.14	0.1 ^c	0.07 ^d
Energy Threshold	250 GeV	150 GeV	50 GeV
Field of View (sr)	0.001	0.004	0.004

^a Estimated from Ref. [32].

^b Resolution at 100 GeV [33].

^c Estimated from CAT observations of the CRAB nebula [34].

^d Angular resolution at 300 GeV from simulations of a 4 telescope array [33].

[†] Average quantities estimated for the energy ranges: $E_\gamma > 300$ GeV for Whipple; $E_\gamma > 150$ GeV for GRANITE-III; $E_\gamma > 75$ GeV for VERITAS or HESS

space searching for the annihilation-line flux, if a halo model which provides an increase of the dark matter density towards the galactic center is considered.

In this section we focus on Atmospheric Cherenkov Telescopes (ACTs), such as an upgraded version of the Whipple detector currently under construction (GRANITE-III) as well as proposed arrays of ground-based atmospheric Cherenkov detectors VERITAS [31] and HESS [33]. We will consider in Section 6 the potentiality of the proposed *Gamma-Ray Large Area Space Telescope* (GLAST) experiment. Ground based and satellite experiments are to some extent complementary for our purpose. While satellite experiments offer a lower energy threshold, superior energy resolution, and the possibility of relatively long exposure times, the relatively small effective area ~ 1 m² limits the sensitivity at high energies. On the other hand ACTs offer the potential for very large effective areas ~ 0.3 km², but at a higher energy threshold ($E_\gamma > 250$ GeV).

We summarise in Table 2 the approximate characteristics for existing and proposed ACT gamma-ray observatories.

For the observation of the galactic centre which is treated as a point source, we compute the minimum detectable flux $N_\gamma(E)$ using the prescription that, for an exposure of t seconds made with an instrument of effective area A_{eff} and angular resolution σ_θ (corresponding to a 68% acceptance of events) with corresponding angular acceptance $\Delta\Omega = \pi\sigma_\theta^2$, the conditions for detection are that the significance of the detection exceed 5σ and that

the number of detected photons exceeds 25 events:

$$\text{Significance} = \frac{N_\gamma A_{\text{eff}} t \times 0.68^2}{(A_{\text{eff}} t)^{1/2} (dN_{\text{bg}}/d\Omega \times \Delta\Omega)^{1/2}} \geq 5 \quad (18)$$

$$N_\gamma A_{\text{eff}} t \geq 25. \quad (19)$$

Here, $dN_{\text{bg}}/d\Omega$ is the integral number of background events (per unit solid angle) falling under the annihilation line. If the dominant source of background has a differential spectrum $d^2N_{\text{bg}}/dEd\Omega = N_0 E^{-\delta}$, and if the energy resolution of the instrument is σ_E/E , then the background under a line at energy E_0 (i.e., in the interval $[E_0 - \sigma_E, E_0 + \sigma_E]$ containing 68% of the signal) is given by

$$\frac{dN_{\text{bg}}}{d\Omega} = \frac{N_0}{(\delta - 1)} E_0^{-\delta+1} \times \eta(\sigma_E/E, \delta) \quad , \quad (20)$$

where

$$\eta(\sigma_E/E, \delta) = \left[(1 - \sigma_E/E)^{-\delta+1} - (1 + \sigma_E/E)^{-\delta+1} \right] \quad (21)$$

gives the the background reduction relative to the integral background spectrum (e.g., $\eta = 0.35$ for an energy resolution of 10%).

Atmospheric Cherenkov detectors employ large (~ 10 m) optical reflectors to image flashes of Cherenkov light from electromagnetic showers formed as high energy γ -rays interact in the earth's atmosphere. The Cherenkov light pool from a γ -ray (at normal incidence) covers an area of roughly 5×10^8 cm² on the ground, and defines the sensitive area of the detector. By making use of the distinctive differences in the shower images, a γ -ray signal can be extracted from the large isotropic background of hadronic showers (e.g. [35]). The point of origin of each shower can also be uniquely reconstructed from the orientation and shape of the shower image to a precision of $\sigma \approx 0.14^\circ$ for a single telescope (e.g. [36]), or roughly a factor of \sqrt{N} better when N telescopes provide stereoscopic views of the same shower image. The total level of detected Cherenkov light is roughly proportional to the energy of the primary gamma-ray shower and provides an energy resolution typically of $\sigma_E/E \approx 20\text{--}40\%$. A further improvement in this energy resolution may be realized with stereoscopic measurements which determine the height of the maximum shower development. Typically observations are made in a differential mode where each observation on-source is followed by an observation of equal duration displaced in right ascension from the source direction, so that the control observations sample the same range of azimuth

and elevation angles. The number of candidate gamma-ray events is taken to be the difference between the number of events passing the data-selection criteria on-source and in the control observations. Using this technique one can determine the two-dimensional distribution of gamma-ray events on the sky, and can reconstruct the energy spectrum of these events assuming that the control region does not contain a significant contribution from diffuse gamma-rays or from a number of point sources.

The energy threshold of atmospheric Cherenkov detectors is determined by the condition that the Cherenkov light signal must exceed the level of fluctuations in the night sky background light. Since both the signal and the background light level are proportional to the mirror area A_m , the signal to noise ratio depends on $\sqrt{A_m}$ and the energy threshold is inversely proportional to this quantity. Since the duration of the Cherenkov pulses is very small (on the order of a few nsec), an additional reduction in the energy threshold can be realized by decreasing the signal integration time. For the largest imaging telescope (the Whipple 10m reflector) the energy threshold is approximately 250 GeV. The use of arrays of telescopes operated in coincidence will result in a larger effective mirror area which when combined with the use of faster electronics and higher resolution cameras will result in a reduction in the energy threshold to perhaps 50 GeV for an array of 10m telescope.

Arrays of telescopes also offer the potential for increasing the effective area and improving the background rejection. N widely spaced telescopes operated independently result in an increase in the effective area by N . As the telescopes are moved closer together, the effective area is reduced but the hadronic rejection can be dramatically improved through better characterization of the shower development with stereoscopic imaging. For the VERITAS (HESS) arrays, 9 (16) 10 m telescopes will be used in a configuration where each gamma-ray event within the sensitive area will result in good shower images in four of the telescopes in the array. In such a mode of operation, we estimate a total effective area of $7 \times 10^8 \text{ cm}^2$ and an additional hadronic rejection by a factor of ~ 4 through improvements in angular resolution and by another factor of ~ 4 through better characterization of the shape of the gamma-ray shower (e.g. Ref. [33]).

The sensitivity of atmospheric Cherenkov detectors is determined by a relatively large background of misidentified gamma-like hadronic showers and from cosmic ray electrons, which dominate at lower energies. The contribution of the diffuse gamma-ray background is included in the sensitivity calculation, but has a relatively steep spectrum $\sim E^{-2.7}$ and does not contribute significantly to the background for atmospheric Cherenkov

telescopes. Even if the diffuse spectrum of the inner galaxy is significantly harder than the cosmic-ray spectrum [37], this conclusion is unchanged.

From data taken with the Whipple 10 m telescope, the measured event rates (after rejection of background) and the effective angular aperture and effective area (determined from Monte Carlo simulations) can be combined to derive the background rate for gamma-like hadronic showers:

$$\frac{dN_{\text{had}}}{d\Omega}(E > E_0) = 6.1 \times 10^{-3} \epsilon_{\text{had}} \left(\frac{E_0}{1 \text{ GeV}} \right)^{-1.7} \text{ cm}^{-2} \text{ sec}^{-1} \text{ sr}^{-1} \quad .(22)$$

The factor of ϵ_{had} is introduced to account for improved hadronic rejection in a future detector compared with the current Whipple detector. As the energy threshold is reduced, the relative efficiency of hadronic showers for producing Cherenkov light is reduced with respect to gamma-ray showers. While this effect would improve the sensitivity at low energies, the background rejection from the image analysis generally deteriorates. For simplicity we have neglected these effects.

The showers initiated by cosmic-ray electrons are indistinguishable from gamma-rays, and these events can only be rejected on the basis of their arrival directions. Cosmic-ray electrons have a steeper spectrum than that of cosmic ray nuclei and become the dominant background at lower energies. From Ref. [38] the integral spectrum for electrons is

$$\frac{dN_{e^-}}{d\Omega}(E > E_0) = 3.0 \times 10^{-2} \left(\frac{E_0}{1 \text{ GeV}} \right)^{-2.3} \text{ cm}^{-2} \text{ sec}^{-1} \text{ sr}^{-1} \quad . \quad (23)$$

(at $E = 250 \text{ GeV}$, the electron flux is a factor of 5 below the hadronic background.)

Combining the hadron and electron background and taking into account the small contribution due to the diffuse gamma ray background, the total background under the annihilation line at E_0 , is

$$\begin{aligned} \frac{dN_{\text{bg}}}{d\Omega} \times \Delta\Omega = & 8.5 \times 10^5 \eta \left[(\epsilon_{\text{had}} + 0.033) \left(\frac{E_0}{100 \text{ GeV}} \right)^{-1.7} + 0.32 \cdot \right. \\ & \left. \cdot \left(\frac{E_0}{100 \text{ GeV}} \right)^{-2.3} \right] \left(\frac{A_{\text{eff}}}{3.5 \times 10^8 \text{ cm}^2} \right) \left(\frac{t}{10^6 \text{ sec}} \right) \left(\frac{\Delta\Omega}{0.001 \text{ sr}} \right) \quad (24) \end{aligned}$$

This can be used together with Eqs. 18 and 19 to derive the flux sensitivity curves of the Whipple atmospheric Cherenkov detector as well as the other proposed detectors, as shown in Figs. 9 and 10.

The Whipple detector is located in the northern hemisphere, and the most likely sites for the VERITAS and HESS arrays are also in the northern

hemisphere (although a southern hemisphere site for the HESS array is being considered). Since the galactic center is a southern source, it transits at large zenith angles for a northern hemisphere observatory (e.g., around 61° at the Whipple site). For such observations at large zenith angles, the point of maximum shower development is more distant than it would be for showers with normal incidence, and the Cherenkov light pool spreads out over a larger area. This has the advantage of increasing the effective area but the disadvantage of raising the energy threshold. For observations of the galactic center at the Whipple site, this results in an increase in the energy threshold and effective area by roughly a factor of 5 [39]. For this reason we do not consider here the CAT telescope which is located at a latitude of 42°N [34] or the HEGRA array [40] which will eventually achieve an energy threshold of 500 GeV at the zenith but a threshold of 2.5 TeV for the galactic center, since in both cases their energy thresholds are too high to be sensitive to the majority of parameter space. The 3.8m CANGAROO telescope in the southern hemisphere [41] has an energy threshold of approximately 1 TeV and will also not probe much of the predicted parameter space. However, the CANGAROO collaboration is currently constructing a 10 m telescope which may eventually be part of an array of telescopes. This would prove to be one of the most important instruments for galactic center observations. Since the details of this proposal are not well established, we consider here a generic “southern array” which has roughly the characteristics of VERITAS. Since a source spends the majority of its time near transit, for such a southern array we do not include the effect of large zenith angle observations on increasing the effective area.

5 Prospectives for the Detection of the Monochromatic γ Line with an ACT

As we have already pointed out, the detection prospectives for the monochromatic γ ray line from neutralino annihilation in the galactic halo critically depend on the profile which describes the dark matter distribution. This is in particular evident for detectors like ACTs which have a small angular acceptance. If a large fraction of the total flux emitted is concentrated in a tiny region of the sky, the galactic center, whose coordinates are known with sufficient accuracy, an ACT can be the ideal instrument for detecting neutralino dark matter. This is true for singular halo profiles. We will show that with the NFW profile, which is not the most singular profile among those that are currently being studied, a signal might be seen already in the

next generation of ACT detectors.

In Fig. 9 (a) and (b) we show the results of the 2γ and $Z\gamma$ line fluxes for the supersymmetric models considered in Section 2 and for the NFW profile which gives the maximal value of $\langle J(0) \rangle (10^{-5} sr)$ in Fig. 8. We have chosen such a small solid angle, which corresponds to the minimal angular acceptance for the observation of a point source for an ACT, because for a singular halo profile the ratio signal to square root of the background increases going to smaller angular acceptances. In the figures we draw also the sensitivity curves for each of the ACT detectors considered in previous section. As can be seen, a significant number of supersymmetric models could give a signal which exceeds the sensitivity of the Southern Array and the VERITAS or HESS detector. The detector in the southern emisphere, having a low threshold (around 50 GeV), explores a region of the MSSM parameter space which may be accessible to other detection methods, in particular to future accelerator experiments. VERITAS or HESS have a higher sensitivity for heavier neutralino masses, in an interval which will be hardly accessible to direct or other indirect detection methods.

As the energy resolution of the typical ACT is not better than around 10%, in the high mass range the two monochromatic 2γ and $Z\gamma$ lines, respectively at the energy $E_\gamma \simeq M_\chi$ and $E_\gamma \simeq M_\chi(1 - M_Z^2/4M_\chi^2)$, are not resolvable. In Fig. 10 we sum the contributions to the flux from the two annihilation processes. As we have pointed out in Section 2, a very interesting feature is that due to $Z\gamma$ annihilation line, the values for the predicted flux are concentrated in a quite narrow band and this clearly enhances the possibility of a discovery.

6 The GLAST satellite detector

In the existing EGRET, and the planned GLAST satellite experiment, high energy gamma-rays interact to form an electron positron pair in a distributed converter/tracker layer. The measured direction of electron and positron in the pair (which improves with increasing energy) and the subsequent electromagnetic cascade in the calorimeter layer give the arrival direction and energy of each gamma-ray. An anticoincidence shield effectively rejects background cosmic-ray nuclei and electrons, and the sensitivity of these detectors is limited only by counting statistics and by the diffuse gamma-ray background.

For an energy resolution of 4%, an angular resolution of 0.1° (at $E_\gamma > 10$ GeV) it is clear that the limit given in Eqs. (18) and (19) applies for the

point source sensitivity, and that such observations are counting-statistics limited. Given this fact it is advantageous to change the observing strategy and to relax the angular acceptance window in order that the number of collected gamma-rays is increased above the threshold for detection (around 10 events).

The estimate of the diffuse gamma ray background is then crucial to give a prediction for a signal in a satellite based experiment (for ground-based experiments the background from misidentified protons is generally higher). The diffuse emission of gamma rays in the galaxy is thought to be due mainly to cosmic-ray protons and electrons interacting with the interstellar medium, and has an overall enhancement towards the inner galaxy and the galactic disk. Given that the galaxy is essentially transparent to gamma rays up to energies of about 100 TeV, it is possible to derive the gamma ray spectrum in the energy region of our interest from interstellar mass models of the galaxy [42, 43, 44]. This is however beyond the scope of the paper, we will limit ourselves to an order of magnitude estimate which can be obtained extrapolating from existing data at lower energies.

The EGRET experiment has mapped the diffuse gamma ray emission up to about 10 GeV. We assume a power law fall-off in energy in the form:

$$\frac{dN(E_\gamma, l, b)}{dE_\gamma} = N_0(l, b) \left(\frac{E_\gamma}{1 \text{ GeV}} \right)^\alpha 10^{-6} \text{ cm}^{-2} \text{ s}^{-1} \text{ GeV}^{-1} \text{ sr}^{-1} \quad (25)$$

where we have supposed that the normalization factor N_0 depends only on the interstellar matter distribution and is a function of the galactic coordinates (l, b) only. N_0 has been fixed using the EGRET data at 1 GeV published in Ref. [37], in the simple functional form

$$\begin{aligned} N_0(l, b) &= \frac{85.5}{\sqrt{1+(l/35)^2} \sqrt{1+(b/(1.1+|l|0.022))^2}} + 0.5 & \text{if } |l| \geq 30^\circ \\ &= \frac{85.5}{\sqrt{1+(l/35)^2} \sqrt{1+(b/1.8)^2}} + 0.5 & \text{if } |l| \leq 30^\circ \end{aligned} \quad (26)$$

where the longitude l is assumed to vary in the intervall $-180^\circ \leq l \leq 180^\circ$ and the latitude b in $-90^\circ \leq b \leq 90^\circ$. The parametrization is in reasonable agreement with the data at least in the region towards the galactic centre, in which we will use it. The slope parameter α may in principle depend on both energy and the galactic coordinates. We will, however, adopt $\alpha = -2.7$ in lack of data for the energies of interest to us.

6.1 Acceptance and energy resolution

The proposed GLAST satellite detector will have a much smaller area (around 1 m^2) than an ACT. However, the solid angle coverage will be of the order

of one steradian and the energy resolution will be excellent, at the per cent level for gamma rays that enter on the side of the detector and thus pass many radiation lengths of the electromagnetic calorimeter.

As an example [45], the sensitivity of one version of the GLAST calorimeter, consisting of 25 towers (each 32 by 32 cm²) of 10 radiation lengths of CsI, has been simulated using the GEANT program. The geometric acceptance of the instrument was calculated for all gamma rays which fulfil that a cylinder around the electromagnetic shower of more than 18 radiation lengths and a radius of at least two Moliere radii is fully contained within the instrument, giving an energy resolution of better than 1.5% for gamma rays with energies higher than 50 GeV. It was assumed that the diffuse gamma rays enter the instrument from any direction in the upper hemisphere. (as the lower hemisphere will be completely screened by the Earth). This results in a geometric acceptance of 2.1 m²sr.

Taking into account the screening by the Earth of the galactic center region half of the orbiting time, the useful geometric acceptance in a 1 sr cone towards the galactic center is 0.18 m²sr. This is the geometric acceptance both for a monoenergetic neutralino annihilation signal from a region around the center of the galaxy as well as the diffuse gamma ray background, since background photons arriving from other directions can be discriminated by the direction of incidence.

A similar analysis has to our knowledge not been performed for the alternative design SIFTER, but it appears that there the somewhat larger effective area for a given weight of the detector can give a similar improvement of the γ ray line discovery potential [46].

We display in Fig. 11 (a) and (b) the results of the 2γ and $Z\gamma$ line flux from Section 2 using the GLAST parameters just discussed, and assuming a two-year exposure. Also shown is the curve giving the minimum number of events needed to observe an effect at the 5σ level, using Eq. (25) for the galactic diffuse γ -ray background flux. The NFW halo model corresponding to the maximal rate was assumed for the halo.

As can be seen, a fair fraction of our set of MSSM points can be probed under these circumstances. An advantage with a detector of large acceptance is that “clumps” of dark matter of relatively small angular size could still be detected. Since the annihilation flux is proportional to the square of the dark matter density, such enhancements would appear as bright spots on the γ ray sky, without optical counterpart. Another advantage with a satellite experiment is the excellent energy resolution possible, which may enable a separation of the two lines from 2γ and $Z\gamma$ respectively. If both lines were to be observed, a comparison of line strengths would give interesting

information on the supersymmetric model.

If the relative energy resolution is $\epsilon = \sigma_E/E$, the two lines are separable provided that

$$M_\chi \lesssim \frac{M_Z}{\sqrt{4\epsilon}}, \quad (27)$$

which for $\epsilon = 0.015$ gives $M_\chi \lesssim 370$ GeV.

7 Continuum Gamma Rays

Besides the gamma ray line coming from the $\gamma\gamma$ and $Z\gamma$ final states, there may also be produced a continuum γ spectrum mainly from decaying π^0 mesons created in the fragmentation of quarks [47, 48, 49]. The general drawback of the continuum γ spectrum is that in contrast to the γ lines it lacks distinctive features which can exclude other more mundane sources of production if a signal is believed to be found. On the other hand, the number of photons from this continuum source can be much higher than from the line processes.

In fact, should a γ ray line be found, by necessity there has to be a continuum signal also, although in some cases severely affected by the galactic diffuse background. We therefore investigate what can be expected for the higgsino-like high-mass sample, since previous treatments were mainly done for low-mass neutralinos.

For our high-mass sample, the main annihilation mode is into a WW or ZZ pair. We have simulated the continuum photon spectrum from these and $q\bar{q}$ final states through the PYTHIA 6.113 Monte Carlo code [50]. Introducing the scaling variable $x = E_\gamma/M_\chi$, we find empirically that the quantity $x^{1.5}dN_\gamma/dx$ is well described by an exponential in the variable x , as shown in Fig. 12 for $M_\chi = 500$ GeV.

As can be seen, t and b quarks give a quite soft spectrum. Since u quarks (as well as s and d quarks) have a very small branching ratio for these high mass neutralinos, the dominant source of photons above $x \simeq 0.1$ will be WW and ZZ . Both of these final states show a very simple scaling behavior when increasing the energy (i.e. the neutralino mass). This is clearly shown in Fig. 13, where photons from both WW and ZZ at M_χ of both 500 and 2000 GeV can be described to the level of accuracy required for our purpose by the distribution

$$\frac{dN_\gamma}{dx} = \frac{M_\chi dN_\gamma}{dE_\gamma} = \frac{0.73}{x^{1.5}} e^{-7.8x}. \quad (28)$$

The models in our sample with $M_\chi > 300$ GeV with the highest rate of WW and ZZ production have a rate given approximately by

$$(\sigma v)_{WW+ZZ}^{max} \simeq 5 \cdot 10^{-26} \left(\frac{300 \text{ GeV}}{M_\chi} \right)^2 \text{ cm}^3 \text{ s}^{-1}. \quad (29)$$

The observed differential flux at the Earth is then given by

$$\begin{aligned} \phi_\gamma^{\text{continuum}}(E_\gamma) \simeq & 1.2 \cdot 10^{-10} \left(\frac{300 \text{ GeV}}{M_\chi} \right)^4 \frac{dN_\gamma}{dE_\gamma} \cdot \\ & \cdot J(\Psi) \text{ cm}^{-2} \text{ s}^{-1} \text{ sr}^{-1} \text{ GeV}^{-1}, \end{aligned} \quad (30)$$

where $J(\Psi)$ is defined in Eq. (13).

Using the NFW halo profile which gives the highest rate, and integrating over $\Delta\Omega = 10^{-3}$ sr towards the galactic center, this gives the results shown in Fig. 14 for $m_\chi = 300, 500, 1000$ and 2000 GeV. The galactic background curve is the estimate Eq. (25), which for $b, l = 0$ gives

$$\phi_{bkg}^{g.c.}(E_\gamma) \sim 6 \cdot 10^{-5} \left(\frac{E_\gamma}{1 \text{ GeV}} \right)^{-2.7} \text{ cm}^{-2} \text{ s}^{-1} \text{ sr}^{-1} \text{ GeV}^{-1}. \quad (31)$$

We see that below a mass of 1000 GeV, this additional component of the photon spectrum is larger than the estimated background over some energy range, and could thus be observable, see Fig. 15, where also the results for a 50 GeV neutralino (annihilating mainly to $b\bar{b}$) pairs are shown, using the parametrisation of [47] of the γ spectrum from b quarks. As can be seen, at least the 50 GeV candidate would appear to be excluded already by EGRET data, were it not for the uncertainties related to the halo parameters. The combined features of a break in the spectrum and an angular distribution that does not follow that of the disk and bulge of the galaxy could make this type of signal distinguishable from the background, although it may be difficult to exclude other sources of γ rays giving similar features. In fact, present EGRET observations are not inconsistent with a continuum spectrum originating from dark matter annihilations, but other explanations are possible as well [51].

It is interesting to note in Fig. 15 that a 300 GeV higgsino would cause a flatter spectrum than the ‘‘canonical’’ $E_\gamma^{-2.7}$ in the 1 - 100 GeV range. It is intriguing that a flatter spectrum is indeed observed towards the galactic centre, something which has turned out difficult to reproduce in conventional models [52]. Before detection of a line signal it will, however, not be possible to rule out other sources of high energy γ rays. In any case, the

hitherto unexplored energy band between 100 and 300 GeV will be of crucial importance to verify or rule out a supersymmetric component of the γ ray spectrum.

The higher-mass neutralinos (above 1 TeV) do not give as useful a continuum signal because of the rapid decrease with m_χ of the signal (see Eq. (30)), whereas the γ line remains a viable signature up to that region.

8 Discussion

To conclude, we have shown that the new high energy cosmic γ -ray detectors, both ground- and space-based will have an interesting opportunity to search for signals of dark matter particle annihilations in the Milky Way halo. Indeed, existing data from EGRET may already rule out some of the low-mass MSSM models if the halo is of the most singular form studied here.

Even neutralinos as heavy as several hundred GeV could give continuum γ s with an observable flatter spectrum than the $E_\gamma^{-2.7}$ expected in the simplest models of diffuse galactic γ rays, in the direction towards the galactic center. The absence of a clear signature may, however, make an eventual claim of detection of a supersymmetric signal difficult to defend.

The only reliable γ -ray signals indicating directly the existence of slowly moving, heavy neutral particles in the Milky Way halo seem to be the γ -ray lines produced by $\chi\chi \rightarrow \gamma\gamma$ and $\chi\chi \rightarrow Z\gamma$ annihilations. These lines, of intrinsic relative width of the order of 10^{-3} , have no plausible astrophysical background whatsoever and would constitute a “smoking gun” of supersymmetric dark matter.

As we have shown, the larger rates for the line processes found in the recent first full one-loop calculations in the MSSM, together with the central enhancement indicated in simulations of cold dark matter halos, make these processes accessible to the next generation of γ -ray detectors over a fair range of parameters. In particular, if the neutralino is the lightest supersymmetric particle and is heavier than around 1 TeV, detection of the γ line may well be the only way to discover supersymmetry in the foreseeable future, as all other methods (accelerator, direct detection and indirect neutrino detection) are discouragingly far from the required sensitivity.

Acknowledgments

We are grateful to J. Edsö and P. Gondolo for collaboration on the numerical programs used. This work was supported with computing resources by the Swedish Council for High Performance Computing (HPDR) and Paralleldatorcentrum (PDC), Royal Institute of Technology, Stockholm. We thank J. Edsjö for very valuable help with supercomputer runs. L.B. wishes to thank the Swedish Natural Science Research Council (NFR) for support. We are grateful to P. Carlson and T. Francke for helpful discussions on the GLAST calorimeter, and G. Pendelton for information on SIFTER.

References

- [1] See, e.g., K.A. Olive, astro-ph/9712160, to appear in Proc. TAUP97, Nucl. Phys. Suppl., A. Bottino, A. di Credico and P. Monacelli (eds.), in press.
- [2] For a recent review, see, e.g., L. Bergström, astro-ph/9712179, to appear in Proc. TAUP97, Nucl. Phys. Suppl., A. Bottino, A. di Credico and P. Monacelli (eds.), in press.
- [3] G. Jungman, M. Kamionkowski and K. Griest, Phys. Rep. **267** (1996) 195.
- [4] L. Bergström and P. Ullio, Nucl. Phys. **B504** (1997) 27; see also Z. Bern, P. Gondolo and M. Perelstein, Phys. Lett. **B411** (1997) 86.
- [5] P. Ullio and L. Bergström, Phys. Rev. D, in press.
- [6] J. Silk, K.A. Olive and M. Srednicki, Phys. Rev. Lett. **55** (1985) 257; T.K. Gaisser, G. Steigman and S. Tilav, Phys.Rev. **D34** (1986) 2206; S. Ritz and D. Seckel, Nucl.Phys. **B304** (1988) 877; G.F. Giudice and E. Roulet, Nucl.Phys. **B316** (1989) 429; G. Jungman and M. Kamionkowski, Phys.Rev. **D51** (1995) 328; L. Bergström, J. Edsjö and P. Gondolo, Phys.Rev. **D55** (1997) 1765.
- [7] L. Bergström and H. Snellman, Phys. Rev. **D37** (1988) 3737; S. Rudaz, Phys.Rev. **D39** (1989) 3549; G.F. Giudice and K. Griest, Phys.Rev. **D40** (1989) 2549; A. Bouquet, P. Salati and J. Silk, Phys.Rev. **D40** (1989) 3168; F. Stecker and A. Tylka, Astrophys. J. **336** (1989) L51; V. Berezhinsky, A. Bottino and V. de Alfaro, Phys.Lett. **B274** (1992) 122; M. Urban et al., Phys.Lett. **B293** (1992) 149; L. Bergström and J. Kaplan, Astropart.Phys. **2** (1994) 261; G. Jungman and M. Kamionkowski, Phys.Rev. **D51** (1995) 3121.

- [8] R. Carlberg, *Astrophys. J.* **433** (1994) 468.
- [9] J.F. Navarro, C.S. Frenk and S.D.M. White, *Astrophys. J.* **462** (1996) 563.
- [10] A. V. Kravtsov et al., astro-ph/9708176 (1997).
- [11] B. Moore et al., astro-ph/9709051, *Astrophys. J. Lett.*, submitted.
- [12] A. Burkert and J. Silk, astro-ph/9707343 (1997).
- [13] L. Bergström and P. Gondolo, *Astropart. Phys.* **5** (1996) 183.
- [14] J. Edsjö, Aspects of Neutrino Detection of Neutralino Dark Matter (Uppsala University thesis, Uppsala, 1997), hep-ph/9704384.
- [15] P. Gondolo and G. Gelmini, *Nucl. Phys.* **B360** (1991) 145.
- [16] J. Edsjö and P. Gondolo, *Phys. Rev.* **D56** (1997) 1879.
- [17] W. Dehnen and J. Binney, astro-ph/9612059 (1997).
- [18] V.S. Berezinsky, A.V. Gurevich and K.P. Zybin, *Phys. Lett.* **B294** (1992) 221.
- [19] R.A. Flores and J.R. Primack, *Astrophys. J.* **427** (1994) L1.
- [20] T. Fukushige and J. Makino, *Astrophys. J.* **487** (1997) L9.
- [21] N.W. Evans and J.L. Collett, astro-ph/9702085.
- [22] C.S. Kochanek, *Astrophys. J.* **457** (1996) 228.
- [23] D.N.C. Lin, B.F. Jones and A.R. Klemola, *Astrophys. J.* **439** (1995) 652.
- [24] F.J. Kerr and D. Lynden-Bell, *MNRAS* **221** (1986) 1023.
- [25] M.J. Reid, *ARA&A* **31** (1993) 345.
- [26] R.P. Olling and M.R. Merrifield, astro-ph/9711157, to appear in proceedings of the Workshop on Galactic Halos, Santa Cruz, August 1997 (ASP conference Series).
- [27] K. Kuijken and G. Gilmore *Astrophys. J.* **367** (1991) L9.
- [28] A. Gould, *MNRAS* **244** (1990) 25.

- [29] P. Schneider, J. Ehlers and E.E. Falco, *Gravitational Lenses*, Springer-Verlag, Berlin, 1992.
- [30] M.F. Cawley et al., *Exper. Astr.* **1** (1990) 173.
- [31] T.C. Weekes et al., in *Proc. of the 25th ICRC*, 5,(1997) 173.
- [32] P. Goret et al., *astro-ph/9710260*.
- [33] F.A. Aharonian, W. Hofmann, A.K. Konopelko and H.J. Völk, *Astroparticle Physics* **6** (1997) 343.
- [34] A.Barrau et al. 1997, *astro-ph/9705249*.
- [35] P.T. Reynolds, C.W. Akerlof and M.F. Cawley, *ApJ* **404** (1993) 206.
- [36] J.H. Buckley et al., *A&A* **329** (1998) 63.
- [37] S.D. Hunter et al., *Ap. J.* **481** (1997) 205.
- [38] M.S. Longair, *High Energy Astrophysics*, Cambridge U. Press, Cambridge (1992).
- [39] F. Krennrich, *ApJ* **481** (1997) 758.
- [40] N.Bulian et al. 1997, *astro-ph/9712063*.
- [41] T. Kifune et al., in *Proc. of the 4th Compton Symposium, Williamsburg (1997)*, in press, *astro-ph/9707001*.
- [42] D.L. Bertsch et al., *Ap. J.* **416** (1993) 587.
- [43] I.V. Mosalenko and A.W. Strong, *Ap. J.* **493** (1998) in press.
- [44] P. Chardonnet et al, *Ap. J.* **454** (1995) 774.
- [45] L. Bergström, P. Carlson and T. Francke, unpublished.
- [46] G. Pendelton, private communication.
- [47] H.-U. Bengtsson, P. Salati and J. Silk, *Nucl Phys.* **B346** (1990) 129.
- [48] V. Berezhinsky, A. Bottino and G. Mignola, *Phys. Lett.* **B325** (1994) 136.
- [49] P. Chardonnet et al., *Astrophys. J.* **454** (1995) 774.

- [50] T. Sjöstrand, *Comp. Phys. Comm.* **82** (1994) 74.
- [51] D. Dixon et al., as quoted in press release,
<http://tigre.ucr.edu/halo/halo.html>.
- [52] M.Mori, *Astrophys. J.* **478** (1997) 214.

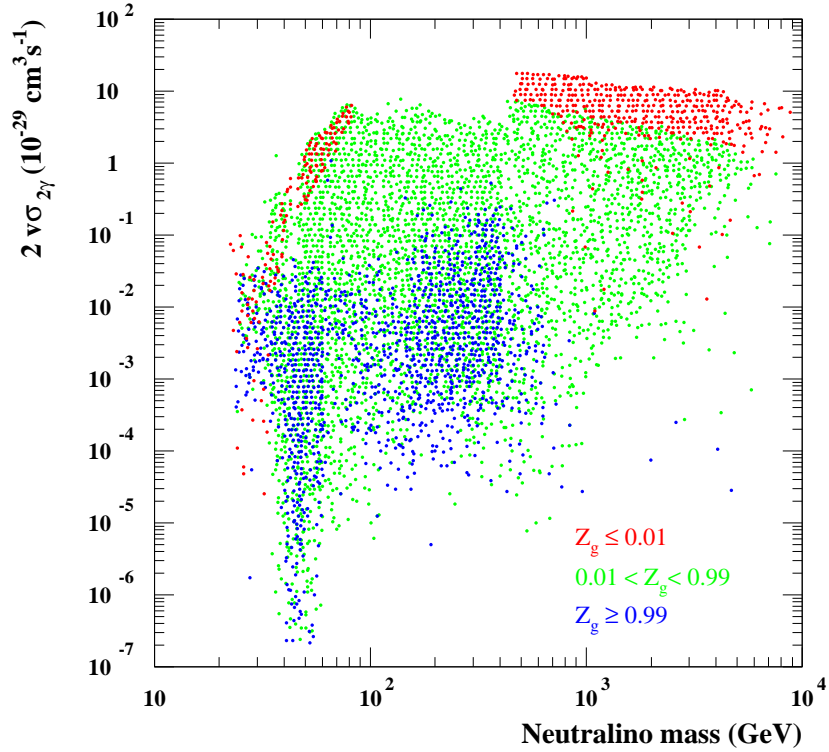


Figure 1: Annihilation rate of neutralinos into the 2γ final state for the sample of supersymmetric models described in Section 2. A different marker color is used for the three classes of neutralinos we have defined: a red marker indicates a higgsino-like neutralino, a green marker a mixed neutralino, while blue markers are for gaugino-like neutralinos.

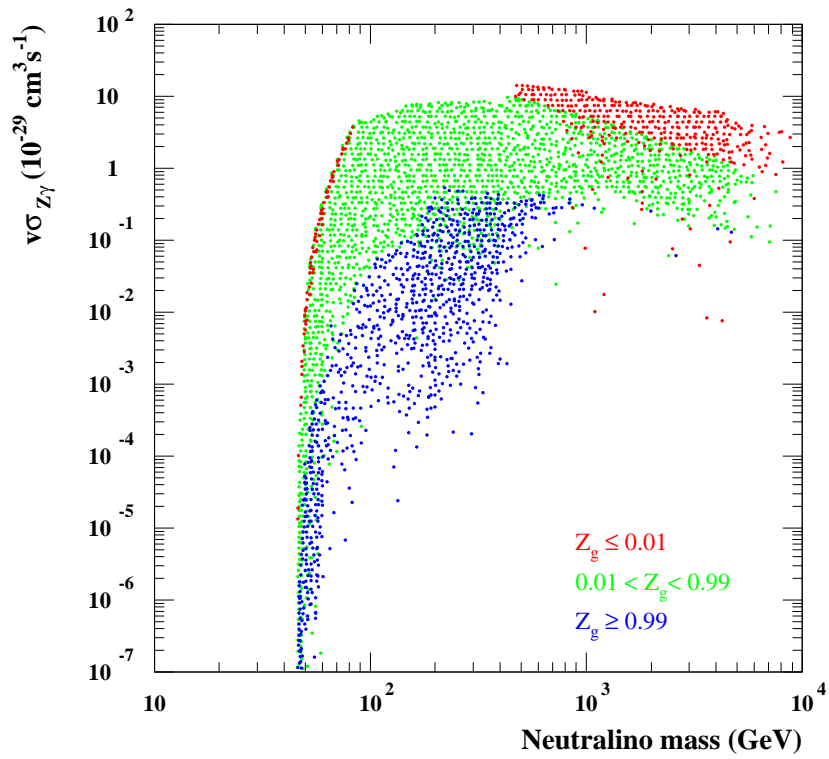


Figure 2: Annihilation rate of neutralinos into the $Z\gamma$ final state for the sample of supersymmetric models described in Section 2. The marker colors have the same meaning as in Fig. 1.

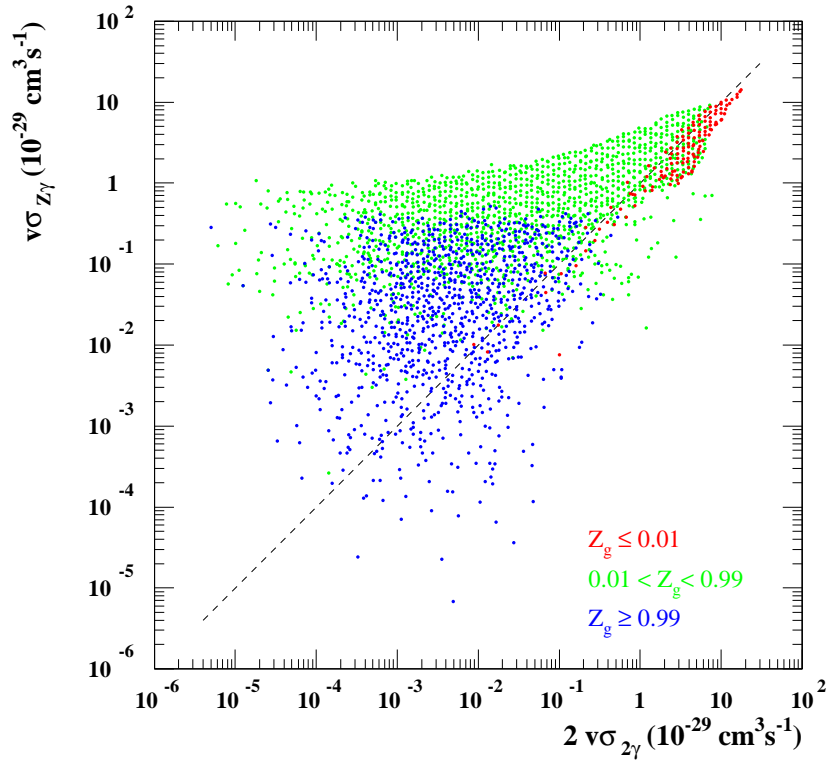


Figure 3: $v\sigma_{Z\gamma}$ versus $2v\sigma_{2\gamma}$ for the sample of supersymmetric models described in Section 2. The marker color has the same meaning as in Fig. 1.

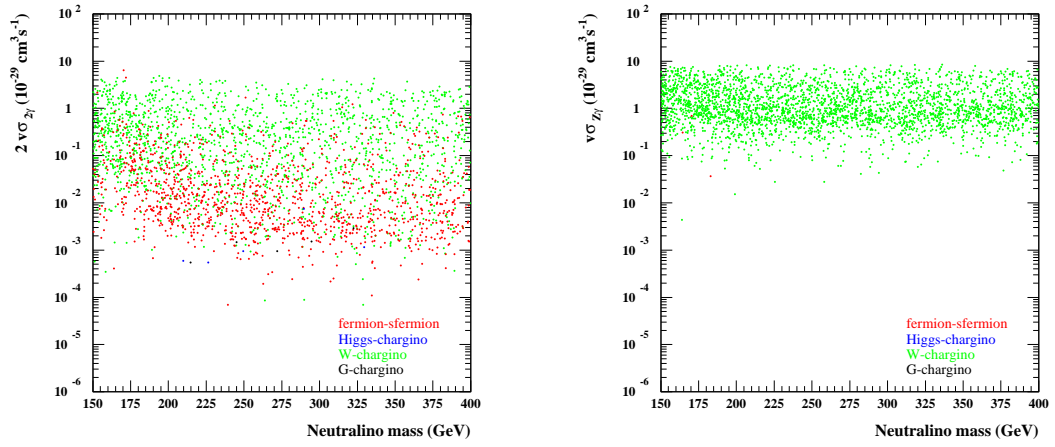


Figure 4: $2v\sigma_{2\gamma}$ and $v\sigma_{Z\gamma}$ for a sample of mixed neutralinos in the mass range 150 - 400 GeV. For each model the class of diagrams which gives the main contribution to the cross section is indicated.

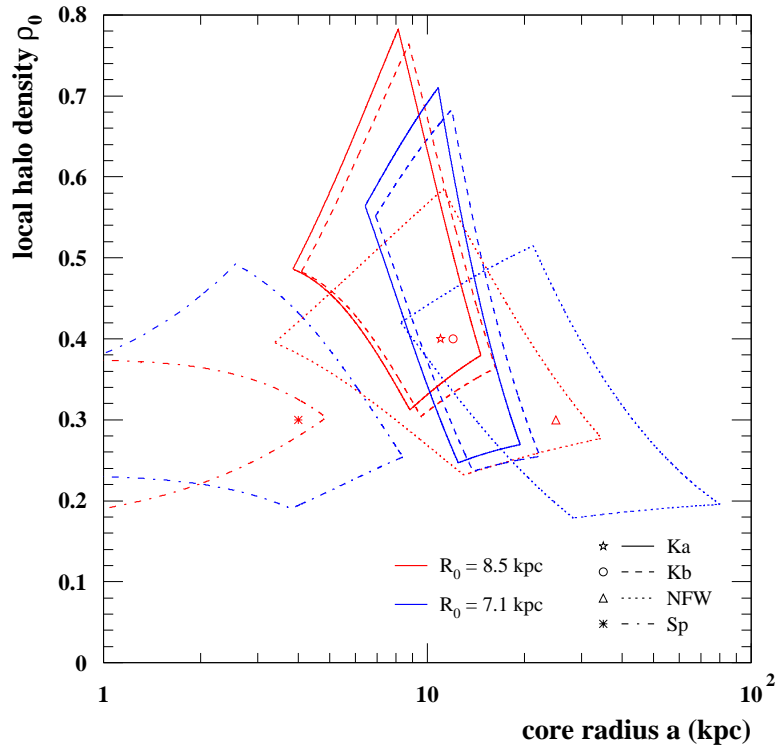


Figure 5: Allowed values of the parameters ρ_0 , the local halo density, and a , the core radius, for the four halo profiles considered in Section 3. The allowed regions vary as a function of the third parameter which enters the discussion, the galactocentric distance of the solar system R_0 ; we plot the regions corresponding to $R_0 = 8.5$ kpc which extend to lower values of a and to $R_0 = 7.1$ kpc which allow higher values of a . The markers indicate the halo profiles which are considered in Fig. 6.

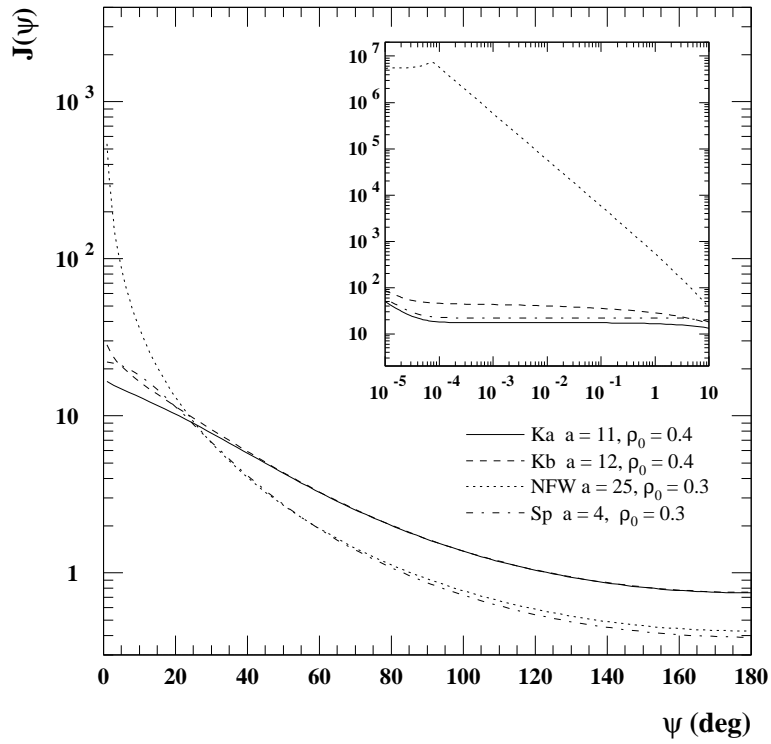


Figure 6: Function $J(\psi)$ as defined in Eq. (13) for the four halo profiles considered in Section 3. The choice of the parameters a and ρ_0 is indicated in the figure, while we have fixed $R_0 = 8.5$ kpc.

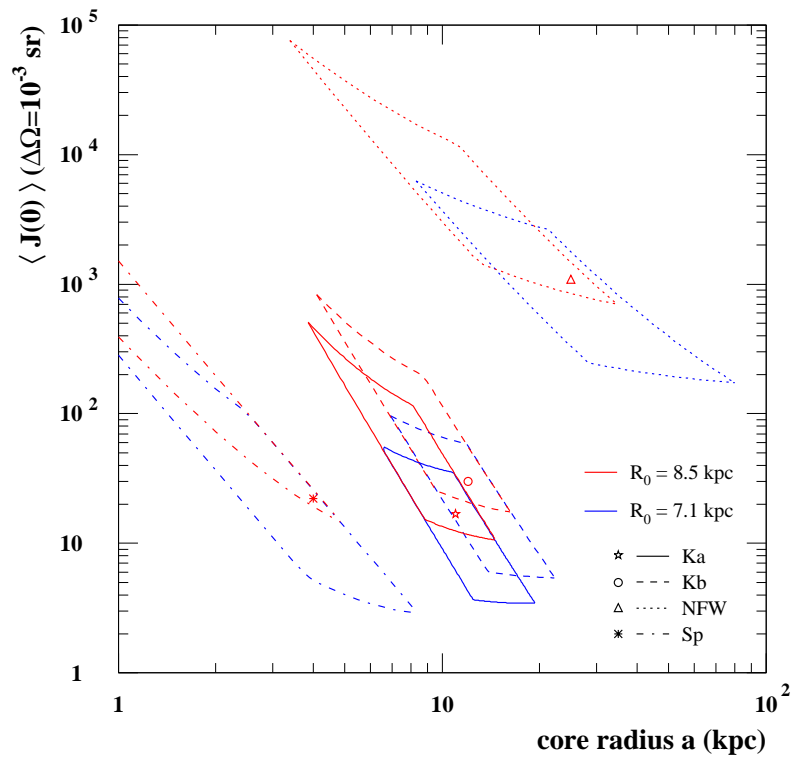


Figure 7: $\langle J(0) \rangle$ as defined in Eq. (14) for $\Delta\Omega = 10^{-3} \text{ sr}$ and as a function of the core radius a for the four halo profiles considered in Section 3. Each contour is given by the maximal and minimal values of the parameter ρ_0 as given in Fig. 5, for the two choices of R_0 .

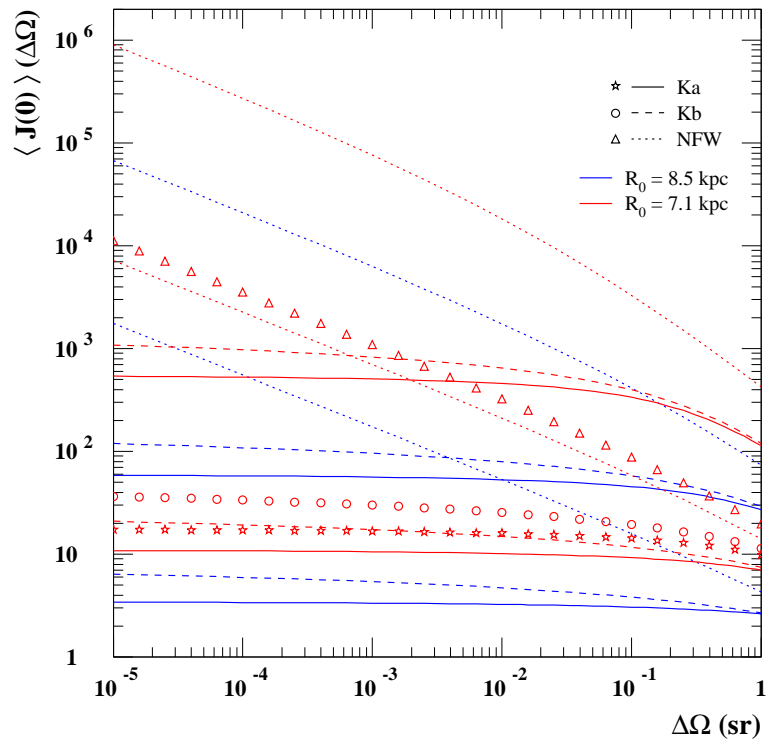


Figure 8: $\langle J(0) \rangle$ as a function of $\Delta\Omega$ for the halo profiles defined by the maximal and minimal values of the core radius allowed in Fig. 5 and for those considered in Fig. 6. Curves for both choices of R_0 are shown.

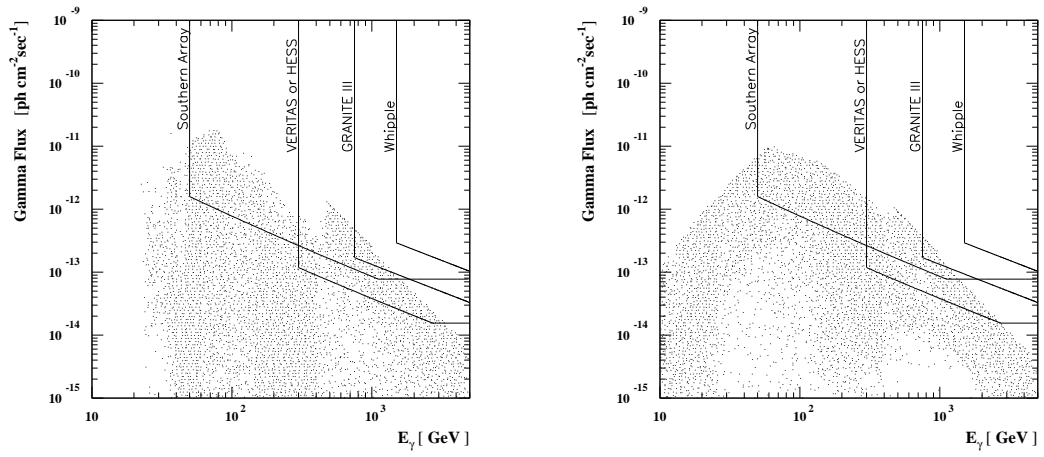


Figure 9: Gamma ray flux from a 10^{-5} sr cone encompassing the galactic center for the 2γ (on the left) and the $Z\gamma$ annihilation line (on the right). The NFW halo profile giving the maximal flux has been assumed. The solid lines show the 5σ sensitivity curves of the ACT detectors described in the text.

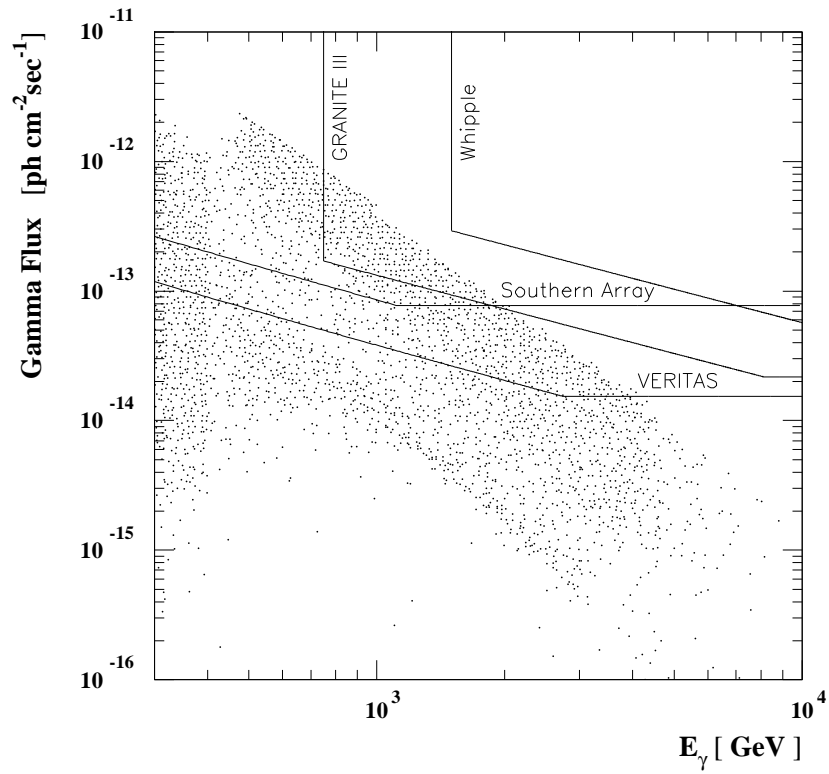


Figure 10: Gamma ray flux from a 10^{-5} sr cone encompassing the galactic center summing the contributions of the 2γ and the $Z\gamma$ annihilation lines for heavy neutralinos. The NFW halo profile giving the maximal flux has been assumed.

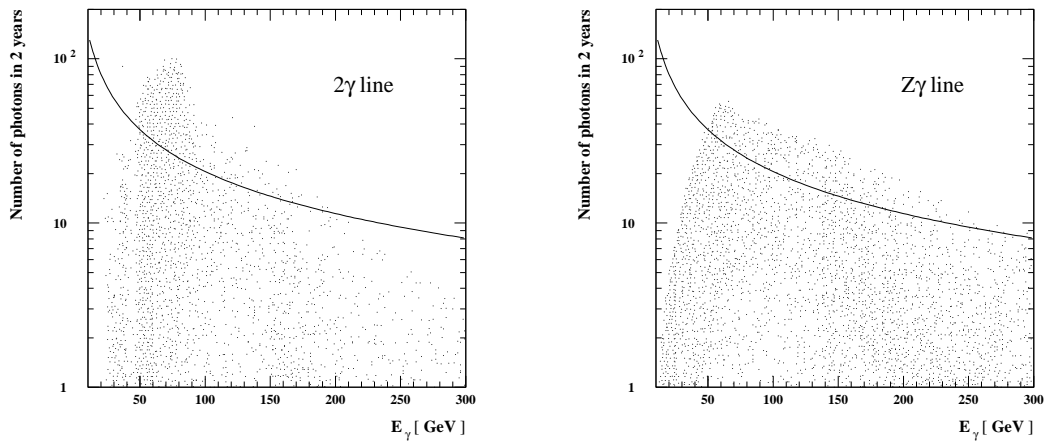


Figure 11: The number of events expected in GLAST from a 1 sr cone encompassing the galactic center, assuming a 2 year exposure and calorimetry as described in the text, for the 2γ (on the left) and the $Z\gamma$ annihilation line (on the right). The NFW halo profile giving the maximal flux has been assumed. The solid line shows the number of events needed to obtain a 5σ detection over the background as estimated from EGRET data.

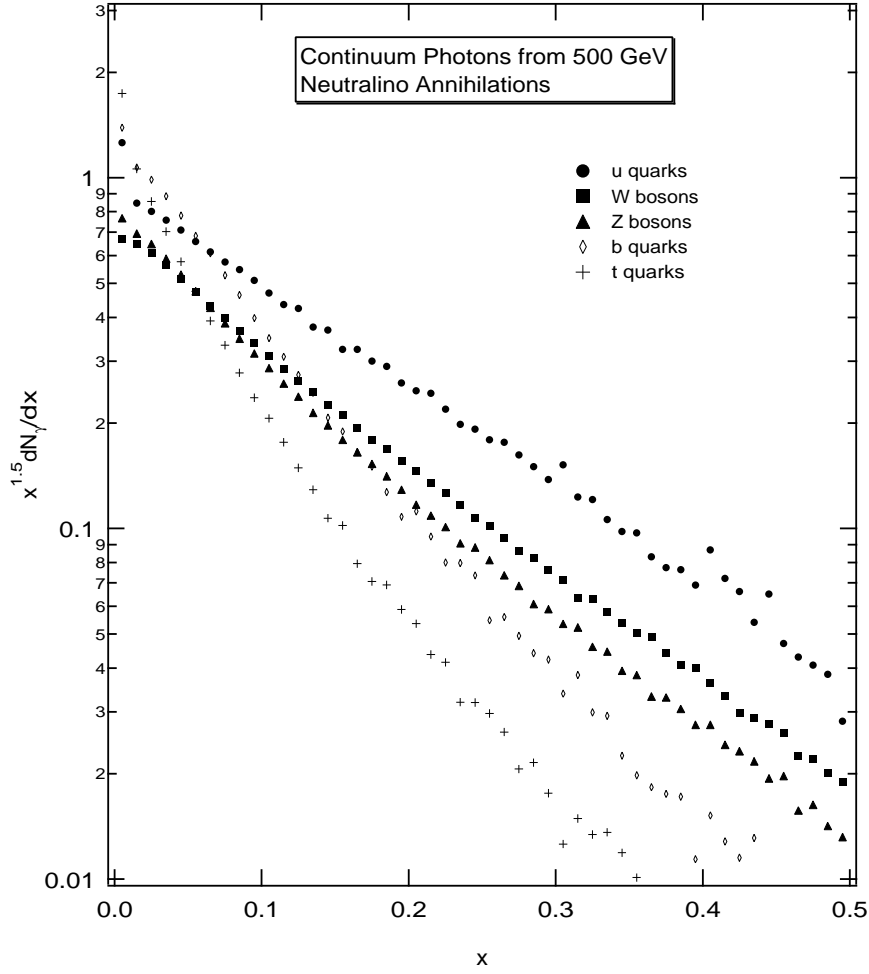


Figure 12: Continuum photons from 500 GeV neutralino annihilations. The rate is given as $x^{1.5}dN_\gamma/dx$ per final state pair for u quarks (filled circles), W bosons (filled squares), Z bosons (filled triangles), b quarks (open diamonds) and t quarks (crosses). The scaling variable x is defined as $x = E_\gamma/m_\chi$, where E_γ is the photon energy and $2m_\chi$ the total energy of the final state in the annihilation. Note that for a realistic neutralino of this high mass, the annihilation into u quarks, normalized to unity in the figure, will generally be much suppressed.

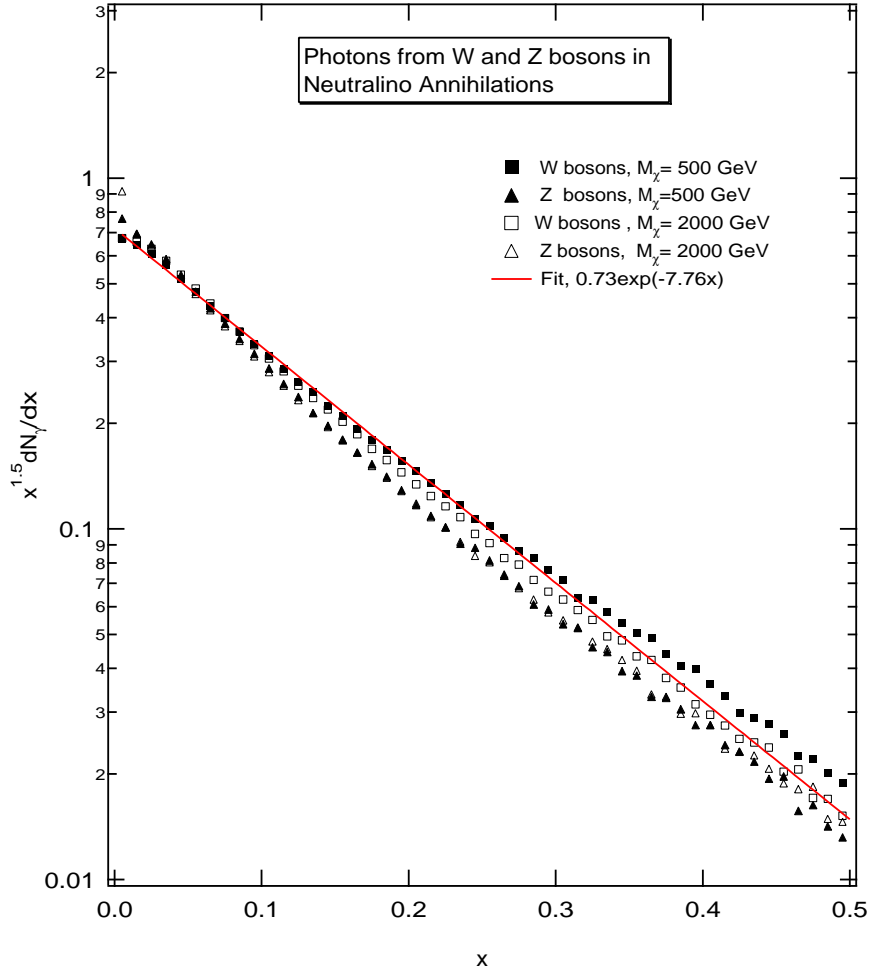


Figure 13: Continuum photons from W and Z bosons in in high-mass neutralino (in practice, mostly higgsino) annihilations. Pythia [50] results for 500 GeV neutralinos are shown with filled symbols, for 2000 GeV with open symbols. The line gives the analytic fit according to Eq. (28).

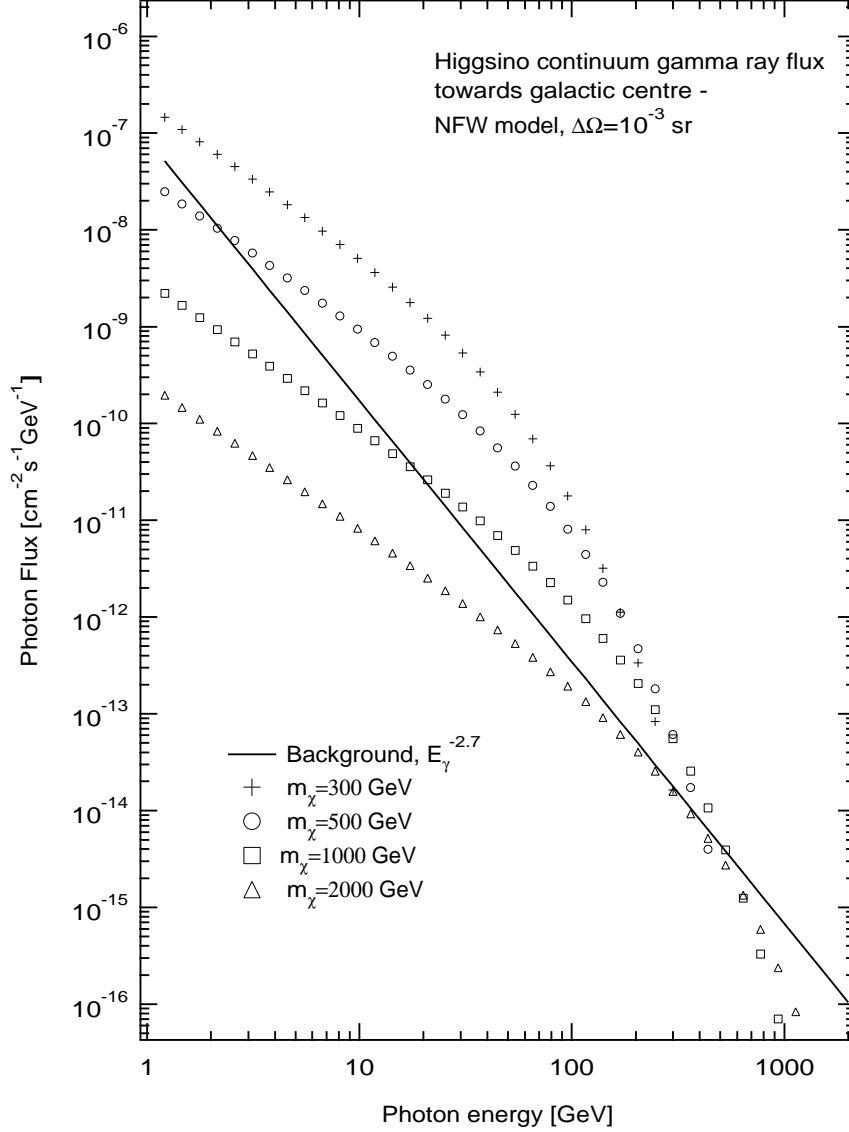


Figure 14: Continuum photons from the direction of the galactic centre originating from W and Z bosons in neutralino annihilations, for $m_\chi = 300, 500, 1000$ and 2000 GeV. The NFW halo profile giving the maximal signal has been assumed, and an angular integration over 10^{-3} sr performed. The background flux (solid line) is that predicted by Eq. (25).

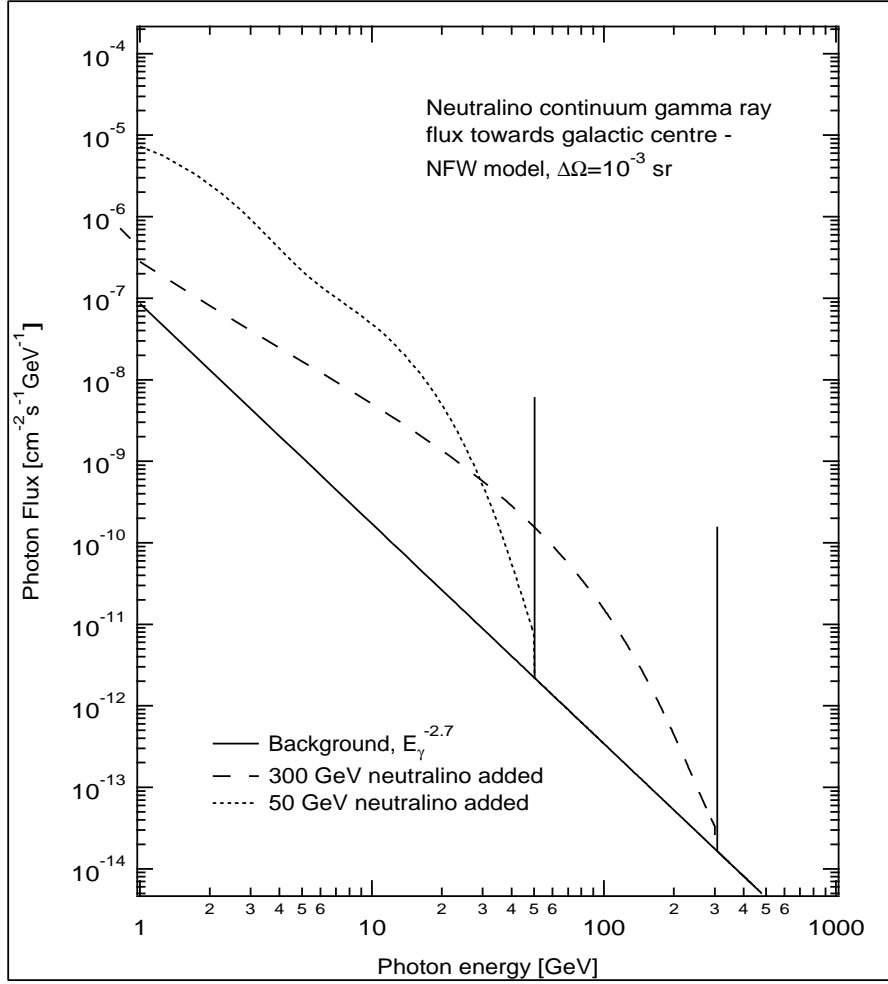


Figure 15: Total photon spectrum from the direction of the galactic centre originating from W and Z bosons in neutralino annihilations, for 300 GeV, and from b quarks for 50 GeV. The NFW halo profile giving the maximal signal has been assumed, and an angular integration over 10^{-3} sr performed. The background flux is that predicted by Eq. (25).

In addition, the maximal γ line strength found in our sample is displayed for these two masses, assuming a relative line width of 10^{-3} .